Fractal Analysis of Zinc Electrodeposition

Chao-Peng Chen and Jacob Jorné

J. Electrochem. Soc. 1990, Volume 137, Issue 7, Pages 2047-2051.
doi: 10.1149/1.2086862

Fractal Analysis of Zinc Electrodeposition

Chao-Peng Chen* and Jacob Jorné**

Department of Chemical Engineering, University of Rochester, Rochester, New York 14627

ABSTRACT

A simple method is proposed for the determination of the fractal dimension during the electrodeposition of zinc by current integration. Under various experimental conditions, 0.01*M* $ZnSO_4$, 2-12V, the patterns formed exhibit scale-invariance characteristics. The fractal dimension of the two-dimensional zinc deposits increases with the applied voltage (or applied current), while the morphology changes from highly branched random aggregate to the radial dense structure. A stochastic model based on the dielectric breakdown model (DBM) is proposed and the simulation analysis indicates that the relative resistivity between the zinc aggregate and the electrolytic solution can play an important role in the pattern transformation. A theoretical model based on the fractal theory is derived to estimate this ratio.

Fractal geometry is an efficient tool for characterizing irregular patterns in very general terms (1). Electrodeposition of zinc has been demonstrated as one of the real physical systems which exhibits a structure similar to the theoretical diffusion-limited aggregation (DLA) model. The observed patterns fall into three classes of deposits: (a) fractals resembling DLA aggregates, (b) dendrites with stable tips, and (c) dense radial structures. The two-dimensional zinc deposits of class (a) bear a striking resemblance to computer-generated fractal patterns and their fractal dimension is 1.7, remarkably close to the computer-simulated value of 1.71 (2). The DLA model has been proposed and discussed by Sander (2), Witten and Sander (3, 4), and Meakin (5). Electrodeposition of zinc fractals was presented by several investigators (6-13) in which the applied potential and electrolyte concentration appear to exhibit a strong influence on the morphology of the zinc deposits. Diffusion to fractal surfaces, electrodeposition of fractals, and computer simulations of electrodeposition and dendritic growth have been treated by Nyikos and Pajkossy (15-17), Voss and Tomkiewicz (18), and Hepel (19). Kahanda and Tomkiewicz (20) examine the evolution of the growth pattern with and without supporting electrolyte. Garik *et al.* (21) discussed the roles of the Laplace and diffusion fields in electrochemical deposition during the growth of the dense-branching morphology.

The fractal (Hausdorff) dimension is usually determined by digitizing photographs and taking the best-fit slope of ln (N) *vs.* ln (r), where $N(r)$ is the number of pixels contained within a radius r (6-8). In the present study we proposed a simpler method which can be used to determine the fractal dimension in a more direct way. The diffusion-limited aggregation model (DLA) has been used to simulate the electrodeposition process. According to this model, ions in the electrolyte undergo a random walk until they reach the cathode. This model does not consider the electric field between the electrodes, and furthermore, it cannot explain the circular envelope of the growing deposits under certain experimental conditions. Therefore, the role of the electric field in the electrodeposition process is still unclear. In this paper, a stochastic model is employed to simulate the deposition process, where the dielectric breakdown model (DBM) and consideration of the electrical resistance among the growing deposits are used to explain the morphology of the zinc deposits. Finally, a theoretical model is derived to estimate the relative resistivity between the deposit and the electrolytic solution.

Experimental

The electrodeposition of zinc and its morphology can be clearly demonstrated in a two-dimensional cell. The cell, as shown in Fig. 1, consisted of a zinc ring anode with diameter of 8.4 cm which was set into a petri dish. Aqueous 0.01*M* $ZnSO_4$ solution was confined into a uniform 0.2 mm film covered by a thin glass. Thin 0.5 mm diam zinc-preplated copper wire, or graphite, was centrally located as the cathode. It is to be noted that a copper ring is not suitable as the anode because codeposition of copper and zinc was observed. A constant potential ranging from 2 to 12V was applied between the anode and the cathode by using a power supply with a voltage regulator designed to compensate the ohmic drop of the shunt, and the corresponding current was measured within ±0.01 mA. In some experiments, constant currents ranging from 0.1 to 1.0 mA were applied while the potential was recorded. During experiments, the radius of the growing deposits was monitored under an optical microscope and after deposition by using scanning electron microscopy (SEM).

Zinc deposition is affected both by electric migration and diffusion, but mass-transfer limitations were not significant due to the following reasons. The cell gap used in the experiments was very thin, on the order of 0.2 mm, and was sandwiched by two insulators, the top thin glass plate and the bottom acrylic cell body. The zinc deposit was found to grow preferentially in the radial direction and the moving boundary of the growing deposit was so fast that the deposition process was similar to the case of a stagnant electrode surface in a well-mixed electrolyte. Furthermore, the low electrolyte conductivity, $1.48 \times 10^{-3}\ \Omega^{-1}\ cm^{-1}$, combined with the concentric configuration

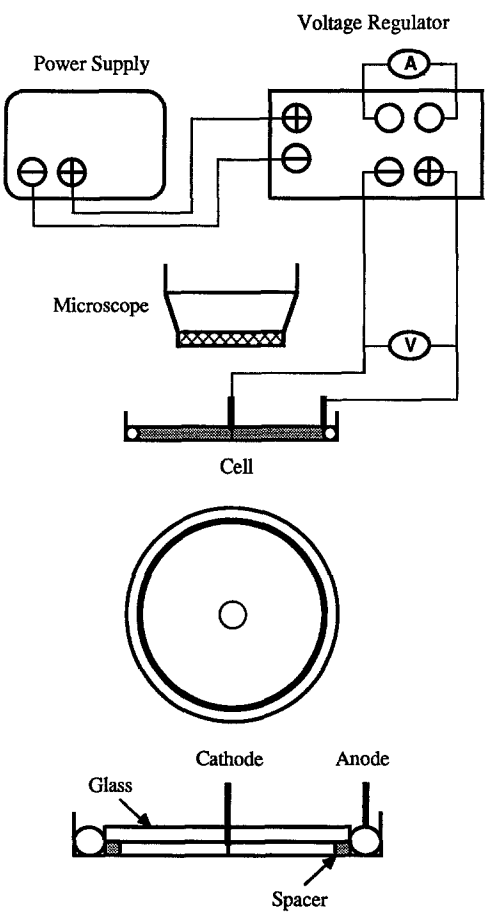

Fig. 1. Schematic diagram of the electrodeposition system

* Electrochemical Society Student Member.
** Electrochemical Society Active Member.

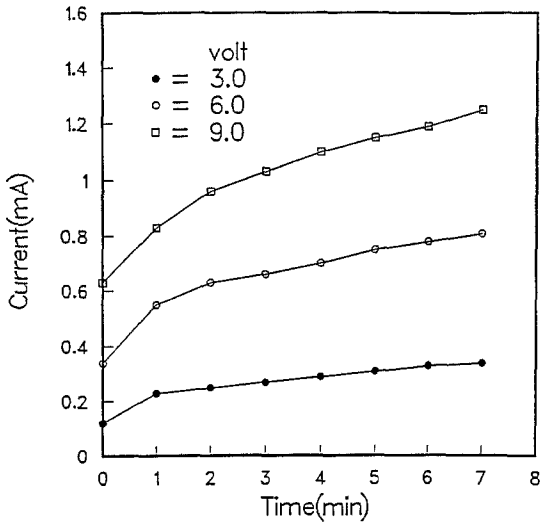

Fig. 2. Current vs. time for zinc electrodeposition under various applied potentials.

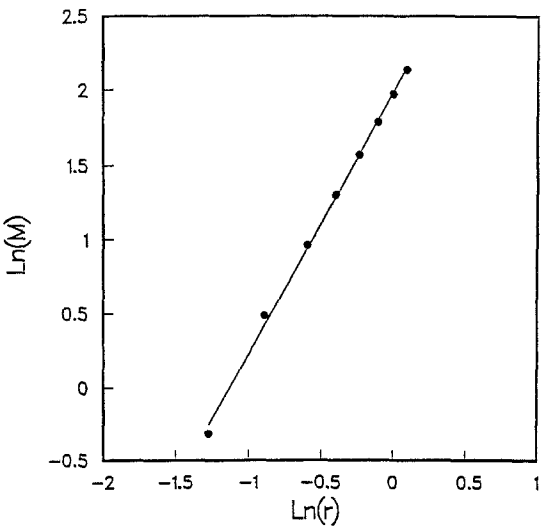

Fig. 4. Logarithmic plot of aggregate mass vs. its radius under applied potential of 9V. $D_f = 1.75$.

of the cell, made the electrodeposition of zinc to be ohmic-controlled.

Results and Discussion

Determination of zinc fractal dimension.—The fractal structure can be characterized by the equation

$$M(r) \sim r^{D_f} \quad [1]$$

where $M(r)$ is the mass of the aggregate within the radius r and D_f is the so-called fractal dimension. Figures 2 and 3 show typical current and growth curves, respectively, during zinc electrodeposition. Figure 2 can be integrated to obtain the mass-time curve by using Faraday's law. Then by logarithmically plotting the mass of the deposits *vs.* their radius, the fractal dimension can be obtained from the slope of the best-fit straight line, as shown, for example, in Fig. 4. The results show that the patterns formed exhibit scale-invariance characteristics under the experimental conditions. Similar results have been obtained by Brady and Bell (9) for copper electrodeposition in a three-dimensional system, $D_f = 2.43$. In this region, the morphology of the aggregates has been classified as the DLA-type. Figure 5 shows the dependence of the fractal dimension on the applied potential, while the morphology of the electrodeposit changes from the highly branched random aggregate to the radial dense structures, as shown in Fig. 6. This method is valid only when the current efficiency is 100%. No competitive reaction such as hydrogen evolution was observed under the optical microscope during the zinc electrodeposition, and the current efficiency approached 100%. Current efficiencies were determined by titration of the zinc deposits with dilute sulfuric acid and comparison to current-time data. Similar behavior was obtained under galvanostatic operation in which various constant currents, rather than potentials, were applied between the growing aggregate and the ring anode. Figure 7 shows the dependence of the obtained fractal dimensions on the applied current for the galvanostatic experiments. In both modes of operation, the surface area of the growing deposit increased significantly with time; thus, current densities cannot be calculated based on the initial area of the central electrode.

In electrolytic solutions, the diffusion length, $\lambda = \sqrt{2Dt}$, is very small, on the order of 0.1 cm; thus, if the deposition process is diffusion-limited, then the deposition should be limited to the electrolyte in the immediate surrounding of the aggregate. However, according to our analysis, the mass deposited is much larger than the original mass of zinc ions within the aggregate. Consequently, the electrical migration of the ions dominates the process, and the dimension of the aggregate is larger than that of the DLA, especially under higher applied potentials.

Computer simulation of zinc fractal.—A computer simulation using the dielectric breakdown model (14) is proposed to explain the morphological changes and the variation of the fractal dimension during zinc electrodeposition.

Like the real system, a point cathode with zero potential, $\phi = 0$, was set at the center of the circular anode, $\phi = 1$, as

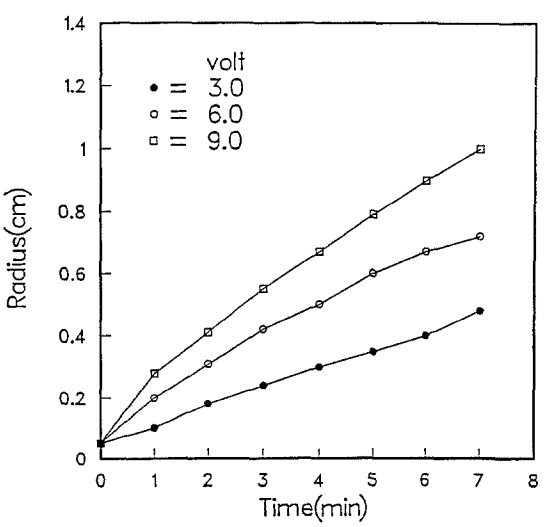

Fig. 3. Growth of zinc aggregate: radius vs. time under various applied potentials.

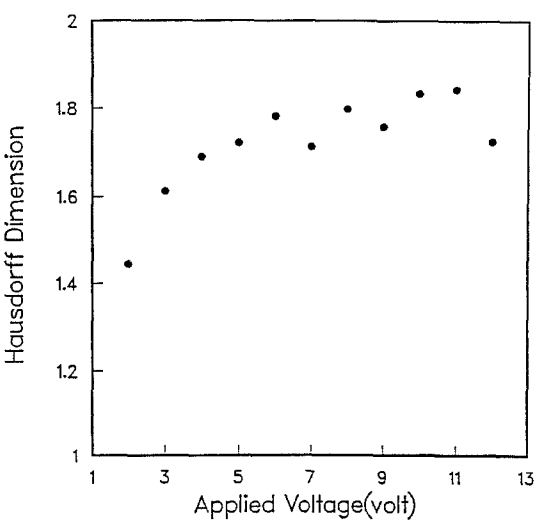

Fig. 5. Fractal dimension vs. applied potential for zinc electrodeposition from 0.01M $ZnSO_4$ solution under potentiostatic condition.

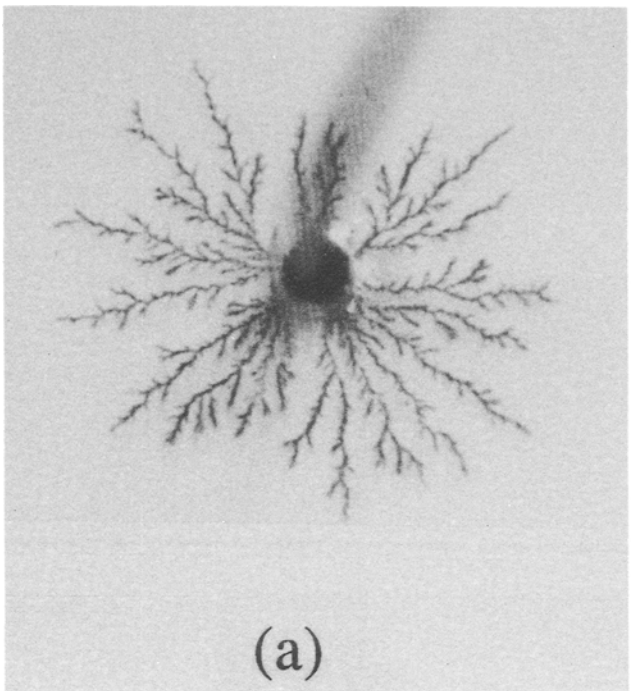

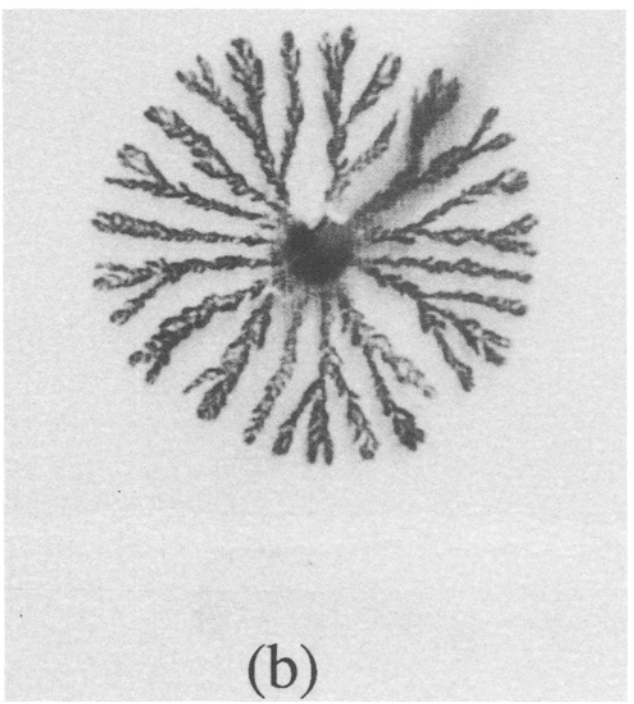

Fig. 6. The morphology of zinc electrodeposited from 0.01M $ZnSO_4$ solution under various applied voltages: (a) $V = 2V$; (b) $V = 8V$.

shown in Fig. 8. The space was discretized into square lattices, so that each point has four neighbors and any two points are connected to each other by a resistor with conductivity κ_i or resistivity ρ_i. The deposition process was assumed to be "primary." Thus the potential profile can be obtained by solving the Laplace equation

$$\nabla^2\phi = 0 \qquad [2]$$

The assumption of potential theory without mass-transfer effects has been extensively used and justified by several investigators (7, 8, 12), both from the measurements of the I-V characteristics and the response to a small-amplitude ripple imposed on the dc current. Finite difference method can be employed to calculate the potential distribution between the electrodes. Thus, the Laplace equation now can be written as

$$\phi_{i,j} = \frac{\kappa_{i-1,j}\phi_{i-1,j} + \kappa_{i+1,j}\phi_{i+1,j} + \kappa_{i,j-1}\phi_{i,j-1} + \kappa_{i,j+1}\phi_{i,j+1}}{\kappa_{i-1,j} + \kappa_{i+1,j} + \kappa_{i,j-1} + \kappa_{i,j+1}} \qquad [3]$$

where $\kappa_{i,j}$ is the electrical conductivity between points i and j. In this model, the nearest neighbors of the aggregate were considered as potential candidates for the next deposition. According to Ohm's law, the current density or the deposition rate can be related to the potential gradient between the candidate and the aggregate

$$i = -\kappa\nabla\phi \qquad [4]$$

and a probability function for the electrodeposition can be defined as

$$P(i, j \rightarrow i', j') = \frac{\phi_{i,j} - \phi_{i',j'}}{\sum_{i',j'} (\phi_{i,j} - \phi_{i',j'})} \qquad [5]$$

Given a probability distribution, a new deposit point is then randomly chosen from the pool of candidates. The candidate with higher probability will be preferentially deposited and after each deposition step, the shape of the aggregate is changed and so is the potential distribution. The new profile can be found by using Eq. [3] and an iteration method until the potentials of every point in the system are converged. Since it is believed that the conductivity of the metal aggregate is not so high as that of the metal, a relative resistivity between the deposit and the electrolyte is defined

$$\beta = \frac{\rho_d}{\rho_e} \qquad [6]$$

Figure 9 shows simulation results under various relative resistivities. In the case of Fig. 9a, where β is zero, all the deposit points have high conductivity (*i.e.*, $\phi = 0$), and the evolved pattern shows a highly branched structure. But in Fig. 9b, where $\beta = 0.2$, the electric resistance among the deposit points was considered and the pattern exhibits the disk-type structure. The finite resistance of the deposit seems to play an important role in stabilizing the shape of the growing deposit.

Relative resistivity between the deposits and the electrolytes.—According to the experimental observations, the deposits exhibited a dark black color rather than the normally metallic color, suggesting that the deposit is a powder. If the contact between the powder particles is loose, then the lower magnitude of the resistance introduced is quite possible. Figure 10 microscopically reveals a significant difference in the morphologies of dendrites and powder deposits. In order to estimate the resistivity of the growing deposit, we initially view the pattern as a disk of uniform effective resistivity ρ_d and also assume the whole

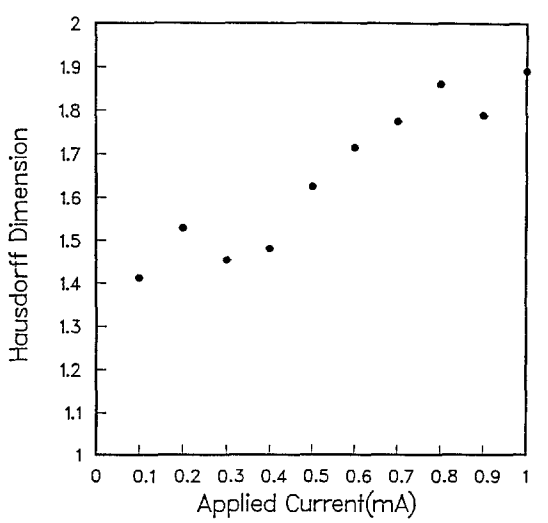

Fig. 7. Fractal dimension *vs.* applied current for zinc electrodeposition from 0.01M $ZnSO_4$ solution under galvanostatic condition.

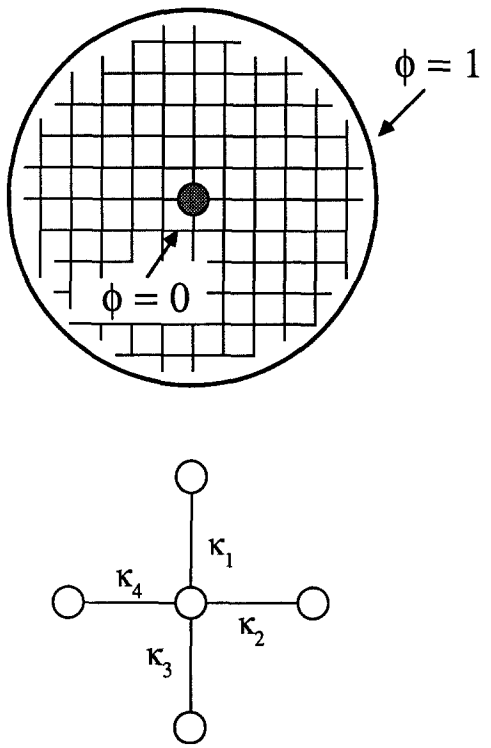

Fig. 8. The stochastic model for the electrodeposition process

process to be "ohmic," as previously assumed by Grier *et al.* (12). The electrolytic cell consists of two concentric cylindrical electrodes separated by an electrolyte. Initially at $t = 0$

$$V_{appl} = \frac{I_o \rho_e}{2\pi L} \ln\left(\frac{r_1}{r_o}\right) \quad [7]$$

and at $t > 0$

$$V_{appl} = \frac{I_t}{2\pi L}\left[\rho_d \ln\left(\frac{r_s}{r_o}\right) + \rho_e \ln\left(\frac{r_1}{r_s}\right)\right] \quad [8]$$

where V_{appl} is the applied voltage, I_o the initial current measured when the power supply just turned on, and I_t the current at time greater than zero. L is the thickness of the electrolyte (*i.e.*, the spacing between plates), r_1 the radius of the circular anode, r_o the radius of the cathode, and r_s is the radius of the growing deposit. Since the experiment was controlled under potentiostatic conditions, these two equations are equal, from which

$$\frac{I_o}{I_t} = \frac{(1-\beta)\ln\left(\frac{r_1}{r_s}\right) + \beta \ln\left(\frac{r_1}{r_o}\right)}{\ln\left(\frac{r_1}{r_o}\right)} \quad [9]$$

By plotting I_o/I_t *vs.* $\ln(r_1/r_s)$, β values can be obtained, either from the slope or from the intercept of the best-fit straight line. However, this model does not consider the electrolyte inside the aggregate. If this factor is taken into account, then some modifications should be made. This is a problem of conduction in heterogeneous medium and we may assume the apparent resistivity of the disk-type pattern to be of the form

$$\frac{1}{\rho_{app}} = \frac{f}{\rho_d} + \frac{(1-f)}{\rho_e} \quad [10]$$

where f is the volumetric fraction of the deposit inside the circular envelope and is a function of radius of the growing deposit. f can be determined from the fractal theory because the deposit shows scale-invariance characteristics (13).

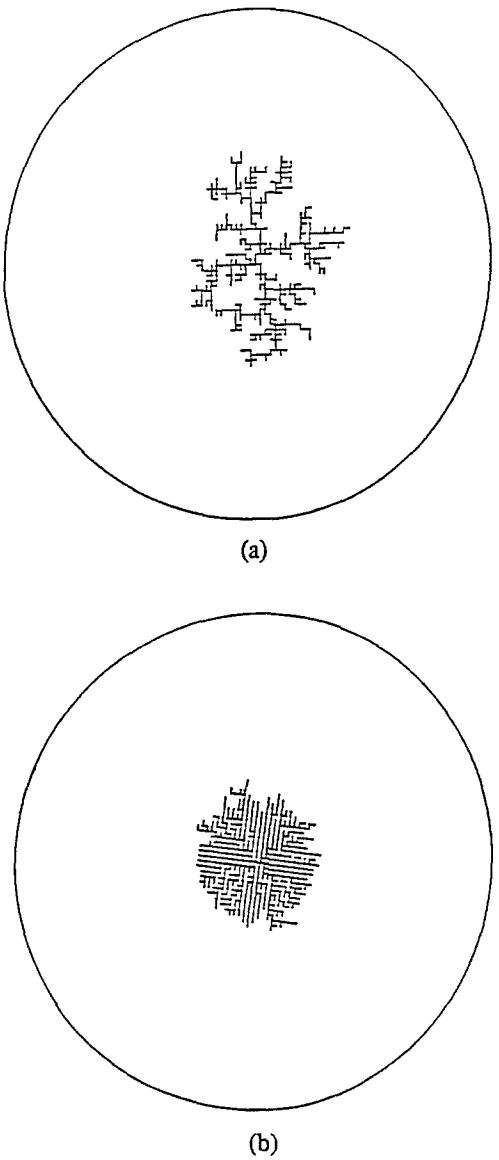

Fig. 9. Computer simulation of zinc fractals under various relative resistivities: (a) $\beta = 0$; (b) $\beta = 0.2$.

For two-dimensional fractal deposits, the mass within a radius r can be expressed as

$$M(r_s) \sim r_s^{D_f} \quad [1]$$

Since the density is defined as $\rho = M/r_s^d$, it is given by

$$\rho(r_s) \sim r_s^{D_f - d} \quad [11]$$

where d is the Euclidean dimension. Accordingly, the solid fraction of the deposit becomes

$$f(r_s) = \frac{\rho(r_s)}{\rho(r_o)} \quad [12]$$

where r_o is the initial radius of the cathode. Substituting Eq. [11] into Eq. [12] gives

$$f(r_s) = \left(\frac{r_s}{r_o}\right)^{D_f - d} \quad [13]$$

Under a potentiostatic condition, the voltage drop between the two electrodes is kept constant at any time, thus

$$\frac{I_o}{I_t} = \frac{\int_{r_o}^{r_s} \rho_{app} \frac{dr}{r} + \int_{r_s}^{r_1} \rho_e \frac{dr}{r}}{\int_{r_o}^{r_1} \rho_e \frac{dr}{r}} \quad [14]$$

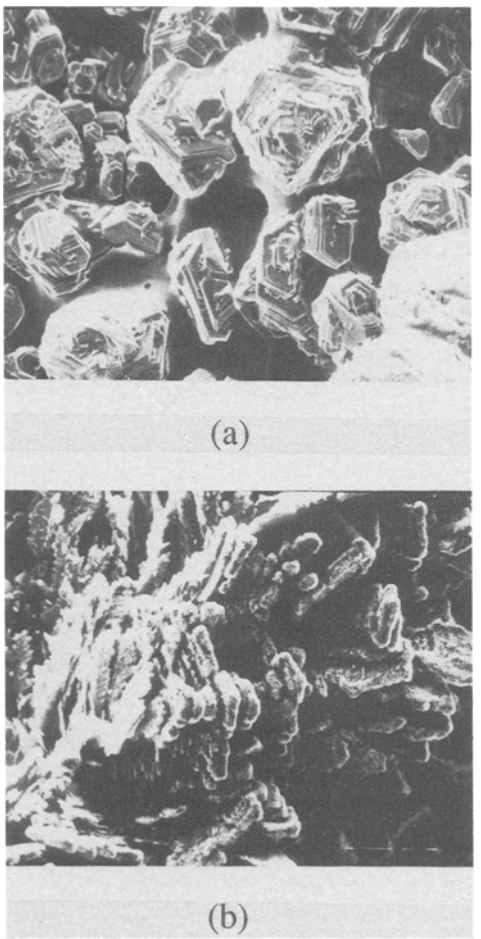

Fig. 10. The microstructures of zinc electrodeposits: (a) zinc crystals; and (b) zinc powder.

Substitution of Eq. [10] and [13] into Eq. [14] gives

$$\frac{I_o}{I_t}\ln\left(\frac{r_1}{r_o}\right) - \ln\left(\frac{r_1}{r_s}\right) = \int_1^{r_s/r_o} \frac{d(r/r_o)}{[(1-\beta)/\beta](r_s/r_o)^{D_f-d+1} + (r_s/r_o)} \quad [15]$$

An explicit form of the solution cannot be obtained for this case and a numerical method, such as Simpson's integration rule and trial-and-error method, is necessary to solve this equation.

Our previous experimental results were taken to test the validity of this model and the results are shown in Fig. 11. The obtained β values vary with the applied potential. This can be explained by the fact that the depletion of the electrolytic solution and the dispersity of the powdery deposits vary with the applied potential. The relative resistivities in Fig. 11 are significantly lower than the value $\beta = 0.132$ reported by Grier *et al.* (12) for radial zinc deposits. Their value seems unrealistically high because the resistivity of the electrolyte is still much higher than that of the zinc deposit, even in its powdery form.

The simulation results qualitatively agree with the experimental data. For $\beta = 0$, the resistivity of the deposit is zero and a branched deposit is obtained. Similar pattern was experimentally obtained under high concentration and under low potential when the deposit showed metallic luster, see Fig. 6a. Disk-like pattern is obtained for $\beta > 0$ when the resistivity of the deposit is significant with respect to that of the solution, see Fig. 6b. Experimentally, such patterns were obtained when the deposits were powdery and lacked metallic luster. The open and highly

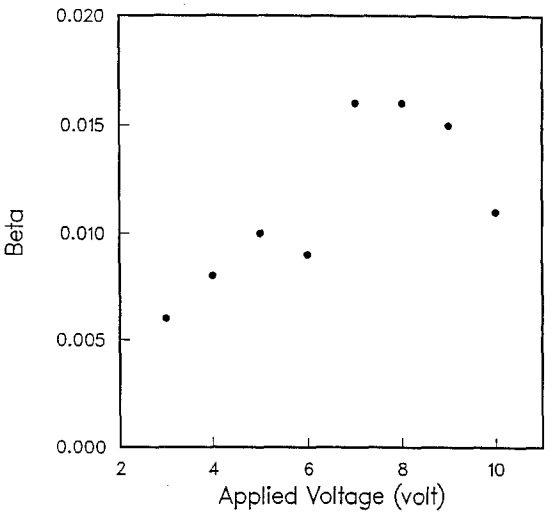

Fig. 11. Relative resistivity vs. applied potential for zinc electrodeposition from 0.01M $ZnSO_4$ solution.

branched pattern can be explained by the Faraday screening effect. The potential gradient inside the aggregate is smaller than that near the outside region, thus the probability is higher there and electrodeposition is preferred near the tips of the branches.

Acknowledgment

Financial support, provided by the National Science Foundation under Grant No. CBT-8518479, is gratefully appreciated.

Manuscript submitted Sept. 14, 1989; revised manuscript received Jan. 25, 1990.

REFERENCES

1. B. B. Mandelbrot, "The Fractal Geometry of Nature," Freeman, San Francisco (1982).
2. L. M. Sander, *Sci. Am.*, **256,** 94 (1987).
3. T. A. Witten and L. M. Sander, *Phys. Rev. Lett.*, **47,** 1400 (1981).
4. T. A. Witten and L. M. Sander, *Phys. Rev. B*, **29,** 5686 (1983).
5. (a) P. Meakin, *Phys. Rev. A*, **27,** 604, 1495 (1983); (b) P. Meakin, *Phys. Rev. B*, **27,** 5686 (1983).
6. M. Matsushita, M. Sano, Y. Hayakawa, H. Hopjo, and Y. Sawada, *Phys. Rev. Lett.*, **53,** 286 (1984).
7. Y. Sawada, A. Dougherty, and J. P. Gollub, *ibid.*, **56,** 1260 (1986).
8. D. Grier, E. Ben-Jacob, R. Clarke, and L. M. Sander, *ibid.*, **56,** 1264 (1986).
9. R. M. Brady and R. C. Bell, *Nature*, **309,** 225 (1984).
10. D. Bensimon, E. Domany, and Aharoni, *Phys. Rev. Lett.*, **51,** 1394 (1983).
11. E. Ben-Jacob, G. Buetcher, P. Garik, N. D. Goldenfeld, and Y. Lareah, *ibid.*, **57,** 1903 (1986).
12. D. G. Grier, D. A. Kessler, and L. M. Sander, *ibid.*, **59,** 2315 (1987).
13. C. P. Chen and J. Jorné, Abstract 324, p. 473, The Electrochemical Society Extended Abstracts, Chicago, IL, October 9-14, 1988.
14. L. Niemeyer, L. Pietronero, and H. J. Wiesmann, *Phys. Rev. Lett.*, **52,** 1033 (1984).
15. L. Nyikos and T. Pajkossy, *Electrochim. Acta*, **30,** 1533 (1985).
16. L. Nyikos and T. Pajkossy, *ibid.*, **31,** 1347 (1986).
17. T. Pajkossy and L. Nyikos, *This Journal*, **133,** 2061 (1986).
18. R. F. Voss and M. Tomkiewicz, *ibid.*, **132,** 371 (1985).
19. T. Hepel, *ibid.*, **134,** 2685 (1987).
20. G. L. M. K. S. Kahanda and M. Tomkiewicz, *ibid.*, **136,** 1497 (1989).
21. P. Garik, D. Barkey, E. Ben-Jacob, E. Bochner, N. Broxholm, B. Miller, B. Orr, and R. Zamir, *Phys. Rev. Lett.*, **62,** 2703 (1989).